SPACE TELESCOPE SCIENCE INSTITUTE
Operated for NASA by AURA

Instrument Science Report STIS 2007-04

wx2d: A PyRAF Routine to Resample Spectral Images

Linda Dressel, Phil Hodge, & Paul Barrett
August 22, 2007

ABSTRACT

Single rows in STIS rectified spectral images are being analyzed in science programs where the highest obtainable spatial resolution is needed. Here we discuss a problem that limits the accuracy of rectified spectral images that contain spatially unresolved components. Because the point spread function is undersampled along the slit, interpolation between the rows of the distorted spectral image to produce an image linearized in the spatial dimension results in errors in the redistribution of the flux. The STScI pipeline and the STSDAS routines calstis and x2d use bilinear interpolation to rectify spectral images. Here we introduce the STSDAS routine wx2d, which iteratively subdivides pixels in the cross-dispersion direction using "average" interpolation of the flux instead of point interpolation, then combines the subpixels into pixels aligned with the spectral trace to form an image that is linearized in the cross-dispersion direction. We compare the products of x2d and wx2d and show that the latter produces substantially smaller errors in the peak flux row of a spatially compact source.

1. Introduction

Artifacts are produced by the rectification of STIS spectral images of targets with spatially unresolved components because the HST point spread function (PSF) is undersampled in the spatial direction. This is especially a problem for the CCD detector, where the FWHM of the PSF along the slit is $\sim$2 pixels. (PSF width as a function of wavelength is quantified for the CCD and MAMA L gratings in ISR STIS 2007-03, Dressel et al. 2007.) For gratings with spectral traces that wander across several rows of pixels as they cross the detector, the artifacts take the form of periodic fluctuations in the row-by-row spectra of the rectified image, which distort or mimic real spectral features. Many STIS spectral imaging programs did not use along-the-slit dithering

to improve the sampling of the PSF in the spatial direction. For these programs, improvements in the rectification of the spectral image depend on improvements in resampling techniques. Here we present iterative "average" interpolation (Barrett and Dressel 2006) as a superior method to bilinear point interpolation for regions of spectral images that contain spatially compact components. The former method is employed by the PyRAF/STSDAS routine wx2d; the latter is used by Calstis and by its constituent routine x2d. The principal advantage of using wx2d is that it can reduce the amplitude of the fluctuations in the peak flux row by a factor of two. More substantial improvements can be achieved using techniques that sacrifice spatial resolution by combining counts from adjacent rows, e.g., by using convolution along columns, an option in wx2d.

Interpolation of spectral images in the cross-dispersion direction is needed to align spectra with rows. In Section 2 of this report, we explain and illustrate how this interpolation produces the patterns that modulate the row-by-row spectra in x2d images of spatially compact targets, and show how the modulation is made worse by the use of spectral traces with the wrong tilt. In section 3, we describe and illustrate how wx2d iteratively subdivides pixels in the cross-dispersion direction using polynomial fits to the integrated flux, optionally convolves the cross-dispersion profile with a PSF kernel, then combines the subpixels into pixels aligned with the spectral trace. Section 4 discusses the task parameters in wx2d and explains how to run the routine and how to apply the best spectral traces. In Section 5, we present two methods of flux calibration of wx2d images, one which interpolates across pixels in the dispersion direction to linearize the wavelength scale (like the routine x2d) and one which preserves the counts per column and reports the non-linear wavelength scale (like the routine x1d). In Section 6, we compare the undersampling-induced modulation patterns produced in row-by-row spectra of a point source by x2d and by wx2d (without convolution) for a variety of values of the wx2d input parameters, which only modestly affect the outcome. We show that, relative to x2d, wx2d reduces the amplitude of the modulation in the peak flux row by a factor of two. We show that the modulation pattern depends on the placement of the target in both the input image and the output image, making it difficult to know what that pattern is in spectral images where it is obscured by complex spatial and spectral structure. We compare the wx2d convolution option to the simple summation of two rows in an unconvolved wx2d image and in an x2d image. The gains achieved by applying superior interpolation techniques to spatially undersampled data are less than the gains that can be achieved by cross-dispersion smoothing (boxcar or convolution) on the scale of the PSF width.

2. Understanding Spectral Artifacts in x2d Images

Artifacts are produced by the rectification of STIS spectral images that contain spatially compact components. Because the spectral traces have structure on the subpixel level and are slightly tilted across the detector, interpolation is required in the cross-dispersion direction to linearize the image spatially. Unfortunately, the point spread

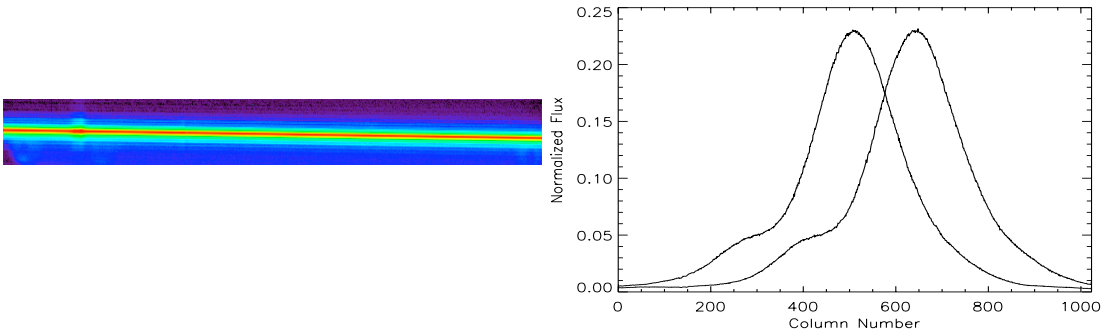

Figure 1: The unrectified spectral image of Beta Lyrae (left, scaled by 2 in y) and a plot of two adjacent rows from this image after normalizing out the stellar spectrum (right).

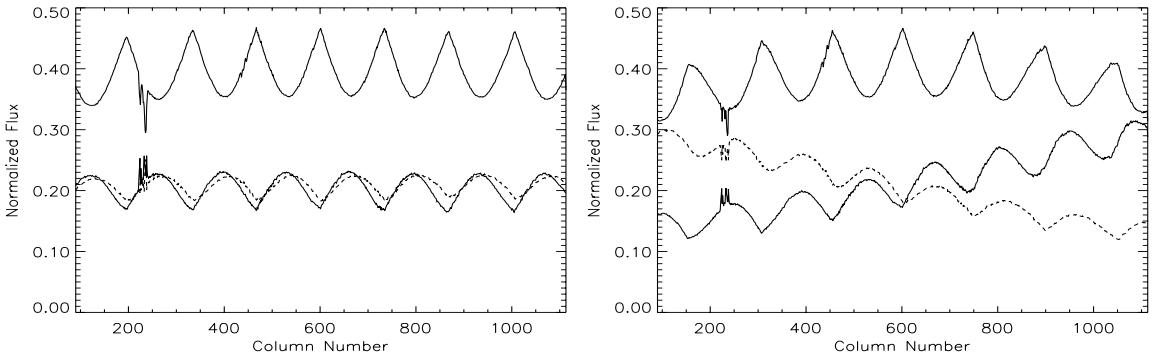

Figure 2: A plot of the peak row and two adjacent rows in the rectified spectral image of Beta Lyrae after normalizing out the stellar spectrum. The rectification was performed by the stsdas routine x2d using a trace derived from the crj image (left) and the obsolete trace reference file l2j0137so_1dt (right).

function is undersampled in that direction, especially by the pixels of the CCD detector. The problem is illustrated in Figure 1. The unrectified subarray image of Beta Lyrae (exposure o5dh01010) obtained with grating G750M(6768) is shown at the left. The flux distribution in two adjacent rows of the image is plotted on the right, after dividing each row by the spectrum obtained by summing over all rows. The flux in one row in the rectified spectrum in the wavelength region between the two peaks will be determined by interpolation between these two flux distributions. The interpolated flux at the cross-over point will be lower than the flux at the peaks.

The interpolation performed by the STSDAS routine x2d, with the spectrum divided out, is shown in Figure 2 for the peak flux row and the adjacent rows. A trace derived from the crj image was used for the plot on the left; an obsolete trace reference file lacking time dependence (l2j0137so_1dt) was used for the plot on the right. The broad structure in the latter plot results from using a trace whose total range in Y is in error by 0.7 pixels. Spectral traces have been found to rotate with time. Also, much of the early calibration of spectral traces was based on exposures taken before changes were made in the settings of the Mode Select Mechanism which positions the gratings.

To avoid the problem illustrated by this figure, one should use traces with calibrated rotation, available for the most commonly used modes in the newest trace reference files, or use the STSDAS routine mktrace to measure and perform the trace rotation for a given science image (ISR STIS 2007-03, Dressel et al. 2007).

The cyclic fluctuations in the plots in Figure 2 occur as the trace drops from one row to the next, and the phase of the interpolation changes continuously. The greatest peaks in the maximum flux row of the rectified image occur where near-integer shifts have been applied to columns where the flux profile was already nearly centered on a row, thus preserving the strongly peaked profile. Between these peaks, the interpolation places too little flux in the maximum flux row and too much flux in the adjacent rows. There are many cycles of fluctuations across the spectrum for gratings with traces that span the greatest number of rows: G230L ($\sim$18), G140M ($\sim$10), G230M ($\sim$16), G430M ($\sim$8), and, shown here, G750M ($\sim$7). (The number of rows spanned by the trace depends on the central wavelength setting, and varies by several rows for the many defined settings of an M grating.)

Summing over 2 or 3 rows of the rectified image greatly reduces the magnitude of the artifacts since they are out of phase in adjacent rows. For gratings with traces that drop or rise by only a fraction of a pixel across the detector, the flux in each row of the rectified image is still modulated by the interpolation errors, but the modulation is much less obvious because it lacks the striking periodicity produced by the strongly tilted traces. For all of the gratings, the flux in each row is also modulated by the wavelength-dependent width of the point spread function. No correction for the PSF is made to the fluxes in x2d images; the counts in each pixel are simply converted to surface brightness if fluxcorr=perform. (See Section 5.4, "Working with Spectral Images", in the STIS Data Handbook, Dressel et al. 2007.) The STSDAS routine x1d makes wavelength-dependent point-source corrections to extracted spectra based on the slit width and extraction box used, but the corrections assume that the PSF does not vary with time, which is not quite correct. (See ISR STIS 2007-03, Dressel et al. 2007).

3. Beyond Bi-linear Interpolation: wx2d

The STSDAS routine x2d uses bilinear point interpolation to rectify spectral images. Early in the operational lifetime of STIS, interpolation using higher order polynomials was tested and was found to produce similar results. More powerful techniques are needed to reduce the errors inherent in resampling undersampled data. Kris Davidson, with the assistance of Kazunori Ishibashi and John Martin, developed a subpixel modelling technique in support of the Hubble Treasury Project to monitor Eta Carinae (Davidson 2005). At STScI, Paul Barrett developed an interpolation routine which iteratively subdivides pixels in the cross-dispersion direction using polynomial fits to the integrated flux, optionally convolves the cross-dispersion profile with a PSF kernel, then combines the subpixels into pixels aligned with the spectral trace (Barrett and Dressel 2005). This routine became the basis of the wx2d routine which we implemented for in-

clusion in STSDAS version v3.6, released in Nov. 2006. It is coded in Python and must therefore be run in PyRAF (http://www.stsci.edu/resources/software_hardware/pyraf) rather than IRAF.

wx2d partitions the counts within each pixel by assuming that an N^{th} order polynomial is a reasonable approximation to the local flux distribution integrated along a column. "Average" interpolation, rather than point interpolation, is used because the flux is distributed over the area of the pixel rather than concentrated at a point. A polynomial is fit to the cumulative distribution of the flux along N pixels, where N is an odd integer. The first point in the distribution, at the leading edge of the first pixel, is zero, and the last (N+1) point is the sum of the flux in the N pixels. For each polynomial fit, the value at the midpoint of the central pixel is calculated. Neville's algorithm is used to find this value because it is fast and accurate. The counts assigned to two subpixels are just the differences between the midpoint value and the points on either side at the edges of the pixel. The algorithm is then repeated to subdivide the subpixels until the desired resolution is reached. Three iterations, yielding eight subpixels from each pixel, has been set as a reasonable default. Optionally, the columns of the subpixeled image can be convolved by a PSF-like kernel at this point. (Note that this convolution is not needed to restore the PSF, since the PSF was not removed in the first place.) Finally, the subpixels are combined into pixels aligned with the spectral trace, with interpolation across subpixels at the outer edges to allow for contributions from fractions of subpixels.

As discussed below, the optional convolution by the PSF-like kernel can be used to reduce the row-by-row undersampling artifacts, but it does this at the expense of contaminating each row with real spectral features from more distant rows in the case of scientifically interesting images with spatial and spectral structure. The kernel has the form $(1 + (x/a)^2)^{-2}$, and approximates the spatial PSF for the STIS CCD L gratings for $a \geq 1.3$ pixels (FWHM ≥ 1.7 pixels). The actual shape of the CCD spectroscopic PSF, which includes a prominent Airy ring, is shown in ISR STIS 2006-02 (Dressel 2006). The typical width of the spatial PSF as a function of wavelength for the CCD, FUV-MAMA, and NUV-MAMA L gratings, and the observed variability of the width, is presented in ISR STIS 2007-03 (Dressel et al. 2007).

The error σ in the flux F in each pixel in a STIS image is stored in the error array, which is in extension [ERR,n] for the n^{th} frame in a file, or extension [ERR,1]=[2] for a single-frame flt file or a crj file. When wx2d distributes the flux in a pixel into two subpixels, it also distributes the variance σ^2 to the subpixels in proportion to the flux:

$F = F_1 + F_2$

$\sigma_i^2 = \frac{F_i}{F}\sigma^2$ for i=1,2

To keep this relationship from giving unreasonable values for very small or negative fluxes, a minimum flux is defined and applied to the computation of the variance:

F_{min} = minimum value of σ in the flt or crj error extension; set to 1 count if this is less than 1 count (as it can be in a MAMA detector exposure)

If $F_1 < F_{min}$ and $F_2 > F_{min}$, then

$\sigma_1^2 = \frac{F_{min}}{F_{min}+F_2}\sigma^2$
$\sigma_2^2 = \frac{F_2}{F_{min}+F_2}\sigma^2$
If $F_1, F_2 < F_{min}$, then $\sigma_i^2 = \frac{1}{2}\sigma^2$ for i=1,2
When the specified number N of subpixels per pixel has been formed, and the subpixels are assembled into new pixels aligned with the trace, the variances associated with the flux in a new pixel are added to form the variance σ^2 for that pixel. (The two fractions of subpixels at the edges of the new pixel are treated as one pixel with the mean variance of the N-1 whole subpixels.) The error σ is recorded in the error array. The Data Quality Index for each new pixel, recorded in extension [DQ,n] for the n^{th} frame, includes every type of quality flag that occurs in the combined subpixels. Since some of the subpixels formed from each of two adjacent pixels will generally be combined into a new pixel, this means that the Data Quality Index for the new pixel includes every type of quality flag that occurred in the original two pixels. When optional convolution with a kernel is performed, only the flux distribution is modified.

The action of wx2d on the flux distribution along the columns of the spectral image of a point source is shown in Figure 3. The source is again Beta Lyrae, observed through the 52X0.5 slit with the G750M grating at central wavelength 6768 Å (exposure o5dh01010). The upper panel of the figure shows flux profiles along the slit in the crj image for a column where the observed trace is centered on a row (black line) and a column where it straddles two rows (green line). The two columns have a small separation in wavelength, so the PSF striking the detector is virtually identical at these columns. (Charge diffusion on the CCD contributes modestly to the difference in the observed flux profiles. See ISR STIS 2006-02 (Dressel 2006) for subpixel modelling and measurement of the PSF.) The central panel of the figure shows how the flux within each pixel is redistributed by wx2d into 8 subpixels for polynomial fits of order 7, using the same color coding as in the upper panel. The symbols and solid lines show the distribution before convolution by the PSF kernel, and the dashed lines show the result of applying a kernel of width 1.3 pixels.

When assembled into pixels centered on the trace, the unconvolved profiles already produce a maximum flux row that is significantly less affected by undersampling artifacts than the maximum flux row of an x2d image, as will be shown below. The periodic fluctuations in the rows of the rectified spectral image disappear as the spatial profiles are convolved to nearly the same shape, but this is clearly achieved at the expense of spatial resolution. Convolution by a kernel approximating the PSF is so effective at producing similar profiles in each column for different input distributions that the improvement achieved by the iterative interpolation is lost when this convolution is used. If each pixel is simply divided into 8 subpixels with the *same* flux (lower panel of Figure 3), the convolved profiles (solid lines) are nearly identical to those in the middle panel (repeated here as dashed lines). The trade-off between maximizing spatial resolution and minimizing spectral artifacts must be considered on a case-by-case basis. While convolution smooths out the spectral baseline provided by an underlying point source in the image of a spatially and spectrally complex region, it also increases the

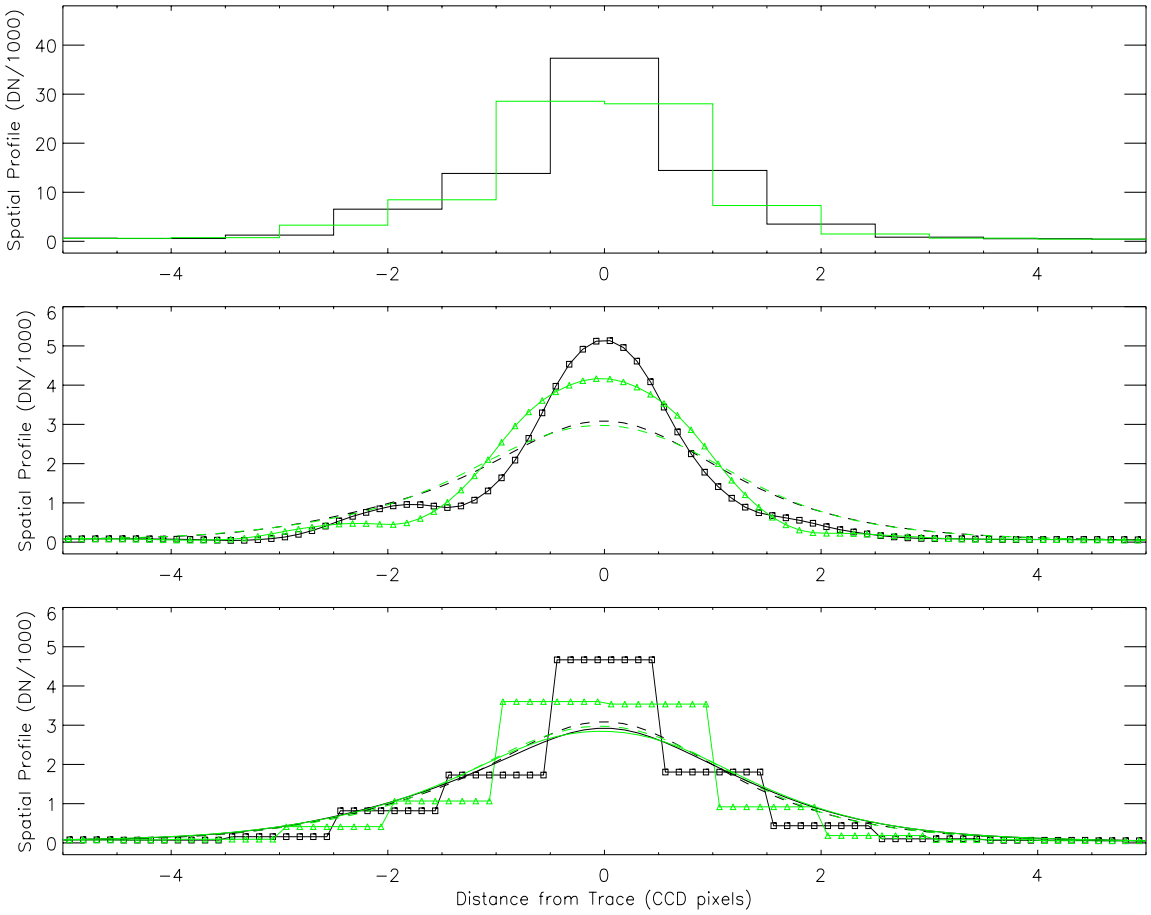

Figure 3: Upper panel: Along-the-slit flux profiles of Beta Lyrae in two columns of the unrectified spectral image, where the trace is centered on a row (black line) and where it straddles two rows (green line). Middle panel: Redistribution of the flux in each column to 8 subpixels using recursive average interpolation (solid lines, color coded as above, with symbols to indicate subpixels) followed by convolution with a PSF kernel (dashed lines, same color coding). Lower panel: Subpixeling without redistribution of the flux (solid lines with symbols to indicate subpixels, color coded as above) followed by convolution with a PSF kernel (solid lines); the dashed lines from the middle panel are repeated for comparison.

cross-contamination of rows with differing spectral features.

4. Running wx2d

The required input parameters for wx2d are the name of an input science image (a flt, sfl, or crj spectral image) and the name of the resampled output image. Optionally, one can produce a wavelength image, where every pixel contains the wavelength of the corresponding pixel in the resampled image, by providing a name for that image. Since no interpolation is done in the dispersion direction, wx2d simply reports the wavelength at a given location on the image, much like the spectral extraction routine x1d. The wavelength image is convenient to use along with the resampled flux image in plotting and analysis languages like IDL. As in x1d and x2d, one can set helcorr to "perform" or "omit" in wx2d to correct (or not) the wavelengths for the velocity of the Earth around the Sun. Calstis or its constituent routine wavecal should be run before running wx2d to populate the keywords SHIFTA1, SHIFTA2 in the science extension(s). The Y-position of the resampled flux image and the wavelengths in the wx2d wavelength image will then be adjusted for the offset of the image from the nominal position on the detector.

wx2d uses the traces in the trace reference file specified in the primary header of the input image (the SPTRCTAB) unless one provides the name of a different trace file; e.g., a newer trace reference file or a reference file generated by the PyRAF/STSDAS routine mktrace. The spectral traces of the commonly used first order observing modes have been found to gradually rotate on the detector over a period of years. The newest trace reference files include parameters that are used by wx2d, x2d, and x1d to rotate the traces to the nominal orientation for the date of the science exposure for these gratings and central wavelength settings: G140L(1425), G230L(2376), G230LB(2375), G430L(4300), G750L(7751), G750M(6581), G750M(6768), and G750M(8561). For any first order grating and central wavelength setting, mktrace can be used to rotate the traces in the SPTRCTAB to the angle appropriate to the science image. The name of the resulting customized trace reference file will be written to SPTRCTAB in the input science image, but the observer may also wish to apply that same customized file to other exposures taken in that visit with the same observing mode and MSM setting.

Other optional parameters for wx2d are the order of the polynomial (default 7) which is used to fit the integrated flux distribution along a column, and the number of subpixels to be produced from each pixel (default 8) by successive divisions of one (sub)pixel into two. One can also specify the width of a PSF kernel to convolve the subpixeled image with (psf_width, default 0 for no convolution, width in pixels using the equation given above). To reduce the computation time, one can select a limited range of rows in the input image to process. The subpixeled images before and after convolution (if psf_width is greater than 0) can be obtained by providing names for them.

5. Flux Calibration of wx2d Images

The resampled image produced by wx2d is in counts. It can be flux calibrated to surface brightness in $erg/(cm^2\ s\ \AA\ arcsec^{-2})$ by running x2d on it with fluxcorr=perform. wx2d sets WX2DCORR to COMPLETE in the primary header so that x2d will recognize that certain corrections have already been applied. x2d thus applies flat traces to the wx2d image, since the image has already been aligned with the traces. It does not apply SHIFTA2, since that offset has already been used to shift the image. x2d uses linear interpolation along rows to convert each row in the wx2d image to the same linear wavelength scale. That wavelength scale can be computed from values of keywords in the header of the science extension of the x2d image as follows:

wavelength = CRVAL1 + (N − CRPIX1) ∗ CD1_1

where N is the column number, CRVAL1 is the wavelength at central column number CRPIX1, and CD1_1 is the linearized dispersion.

Another method of flux calibration can be used to avoid resampling the wx2d image in the dispersion direction, e.g., to preserve spectral resolution or to limit the spread of flux from poorly corrected hot pixels or cosmic ray hits. First, run x2d on the crj or wx2d image with fluxcorr=perform and again with fluxcorr=omit. The STSDAS routine imcalc or the IRAF routine imarith can then be used to compute the ratio of the first image to the second image, which gives the ratio of surface brightness to counts on the linearized wavelength scale. This ratio is the same from row to row, since correction for flats and dark current was performed earlier, and correction for CTI is not attempted. It changes very slowly with wavelength across the bandpasses of the L and M modes, except, in some cases, near the edges of the L mode bandpasses or at the extreme wavelength settings of the M modes. Except at those extremes, an accurate flux calibration can be obtained simply by trimming the ratio image to the size of the wx2d image and multiplying the images together with imcalc.

As an example, perform this procedure for exposure o67117070, a full frame spectral image of the star HD141680 observed with G750M(6581) through the 52X0.2 slit, to produce calibrated flux and error arrays:

wx2d o67117070_crj.fits o67117070_wx2d.fits

x2d o67117070_crj.fits o67117070_x2dcgs.fits fluxcorr=perform

x2d o67117070_crj.fits o67117070_x2dDN.fits fluxcorr=omit

imar o67117070_x2dcgs.fits[1] / o67117070_x2dDN.fits[1] x2d_cgs_per_DN.fits

imcopy x2d_cgs_per_DN.fits[92:1115,88:1111] cgs_per_DN.fits

imcalc o67117070_wx2d.fits[1],cgs_per_DN.fits o67117070_wx2d_cgsflx.fits im1*im2

imcalc o67117070_wx2d.fits[2],cgs_per_DN.fits o67117070_wx2d_cgserr.fits im1*im2

In the upper panel of Figure 4, the red curve shows the sensitivity calibration applied to o67117070_wx2d.fits using the prescription given above. The correct calibration for a given row in the image can be obtained by interpolating that function from

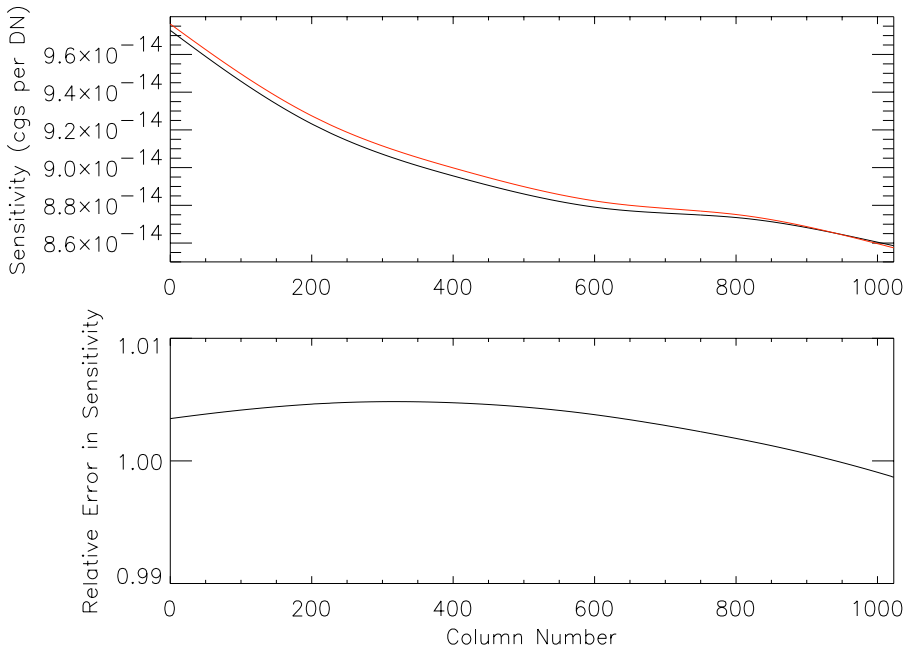

Figure 4: Upper panel: Sensitivity calibration ($erg/(cm^2\ s\ \AA\ arcsec^{-2}$ per DN) versus column number for exposure o67117070 derived using the prescription for producing cgs_per_DN.fits (red line) and adjusted to the variable dispersion of the wx2d image (black line). Lower panel: Ratio of the above curves, to show the relative error in the prescribed calibration method.

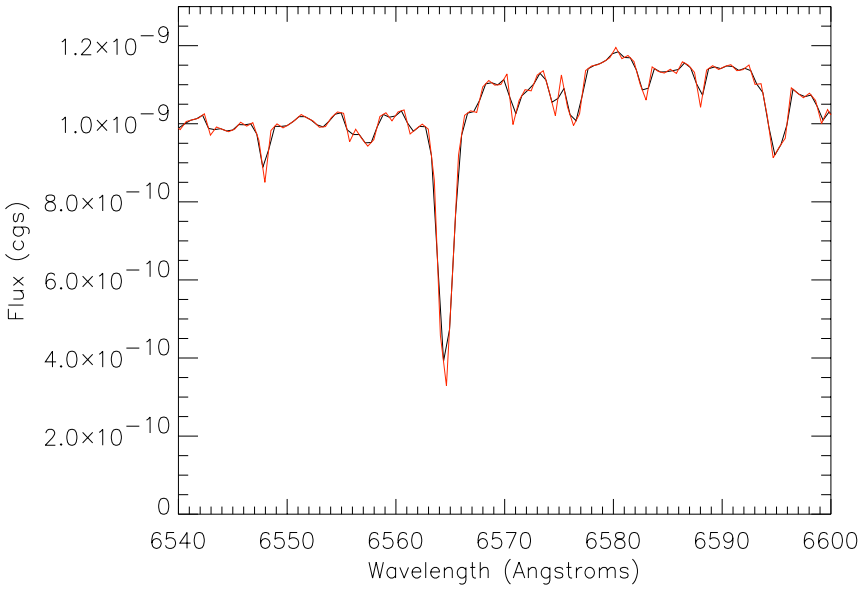

Figure 5: Surface brightness ($erg/(cm^2\ s\ \AA\ arcsec^{-2}$) vs wavelength (Å) from the central row of o67117070_wx2d flux-calibrated by x2d directly (black line) and by the method outlined in the prescription, with no interpolation in the dispersion direction (red line).

the linearized wavelength scale of x2d to the wavelength scale of wx2d along that row, then dividing by the ratio of the variable dispersion in the wx2d image to the dispersion of CD1_1 = 0.554 imposed on the x2d image. The corrected sensitivity curve for the central row of the spectrum in the wx2d image is shown in black. The lower panel of figure 4 shows the ratio of these curves, thus indicating the error in the flux calibration of the prescribed method. In this case, the error is a few tenths of a percent over most of the spectrum, and is virtually all due to the difference in the dispersion in the wx2d and x2d images.

Figure 5 shows part of the central row of the spectrum calibrated in two ways. (A limited wavelength range is plotted so that the small differences in the spectra can be seen.) The red line is from the wx2d image calibrated using the prescription: o67117070_wx2d.fits[1] * cgs_per_DN.fits. The black line is from the image that is obtained by running x2d on the wx2d image with fluxcorr=perform. The visible difference in the two spectra is due to the smoothing applied by x2d when it interpolates along the dispersion direction. This comparison of the spectra produced by the two methods can be used as an empirical check on the relative accuracy of the flux calibration provided by the prescription.

6. Comparison of Artificial Spectral Patterns in x2d and wx2d Images

6.1 wx2d Images Computed with Different Polynomial Orders and Number of Subpixels

Here we compare rows from spectral images of Beta Lyrae (exposure o5dh01010) made with x2d and made with wx2d using several different sets of input parameters. Each row has been divided by the spectrum summed over 21 rows so that the pattern imposed by the resampling can be seen, free of spectral features (except for the residuals of the saturated Hα line). Figure 6 shows the maximum flux row and the next three rows moving down the detector. Figure 7 shows the maximum flux row (again) and the next three rows moving up the detector. Figures 8 and 9 show extracts from Figures 6 and 7, scaled to show the differences between the reductions. In all of the figures, the rows from the x2d image are plotted in black. Three colors are used to show the results of running wx2d with polynomial order 7, assembling the pixels in the final image from 4 (aqua), 8 (blue), and 16 (violet) subpixels. Even in the expanded plots, these lines nearly overplot each other and are difficult to distinguish without magnification (e.g., by zooming the pdf display). That, indeed, is the point. The solutions are not very sensitive to the parameters that have been varied. The lines for 8 and 16 subpixels are virtually identical, showing that subpixeling beyond the default value of 8 is unnecessary. Greater differences are seen when comparing wx2d images made with polynomial fits of different orders. Different colors in the figures show the results of using polynomials of order 3 (green), 5 (red), 7 (blue), and 9 (orange) with the default value of 8 subpixels. The third order fit generally reduces the amplitude of the fluctuations at 2 and 3 rows off-peak, but increases the fluctuations in the peak row.

In all cases, the wx2d images have smaller fluctuations in the central row than the

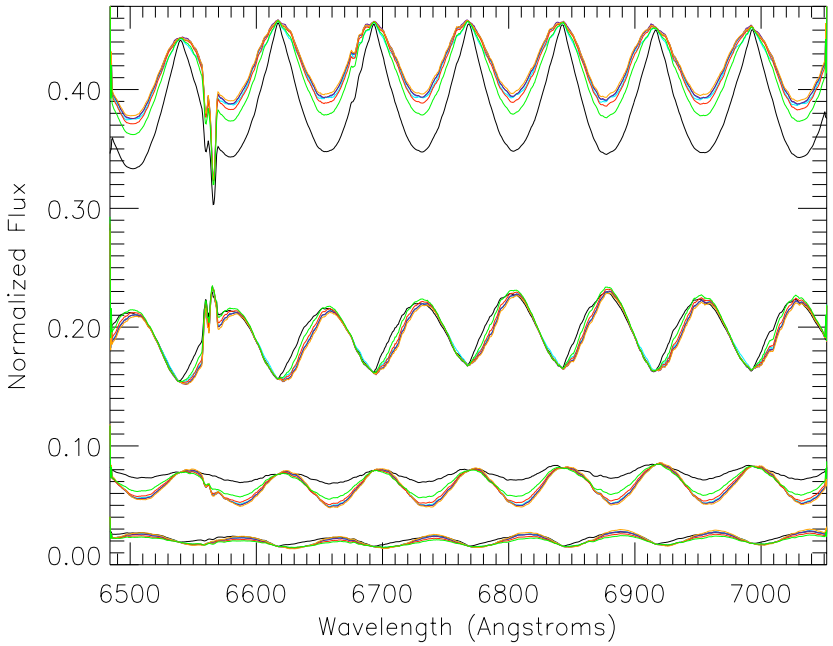

Figure 6: Spectrum in the peak row of o5dh01010 and the next 3 rows down, normalized by the spectrum summed over 21 rows, for reductions using x2d (black) and wx2d for parameters o7s4 (aqua), o7s8 (blue), o7s16 (violet), o3s8 (green), o5s8 (red), and o9s8 (orange), where oN indicates fitting with an Nth order polynomial and sN indicates dividing pixels into N subpixels. (Some lines are difficult to distinguish because the solutions are not very sensitive to the parameters that have been varied.)

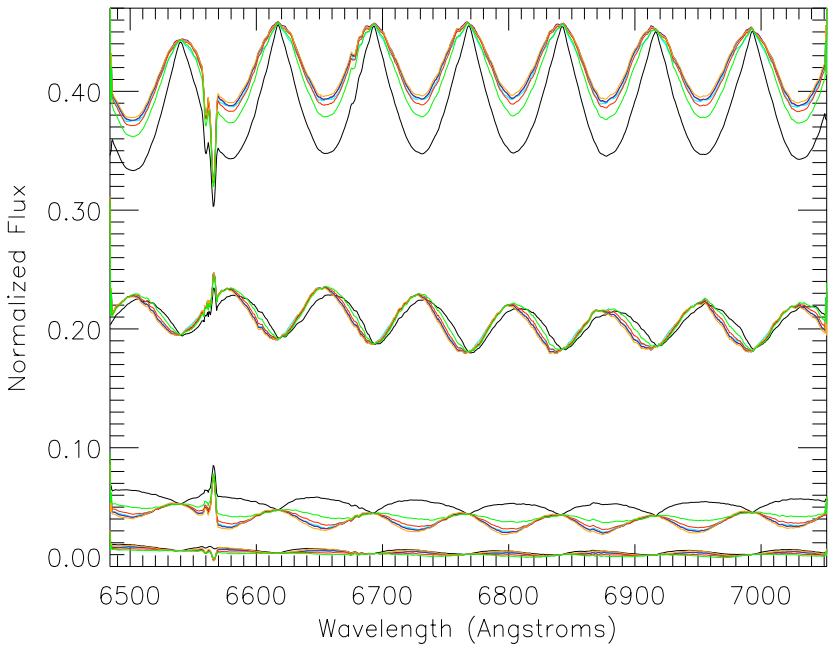

Figure 7: Analogous to Figure 6 for the peak row of o5dh01010 and the next 3 rows up.

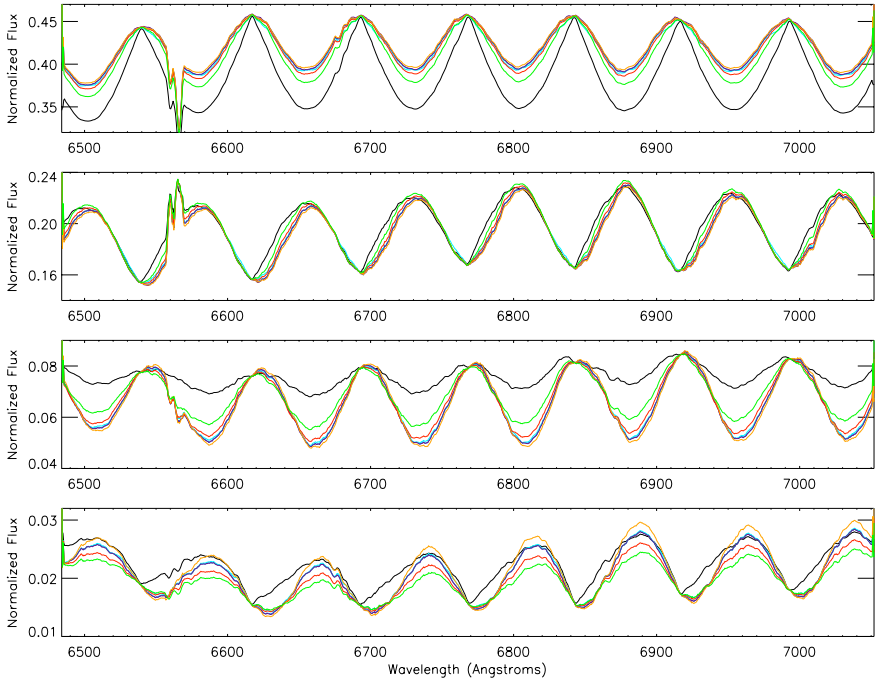

Figure 8: Spectra from Figure 6 rescaled to show structure better.

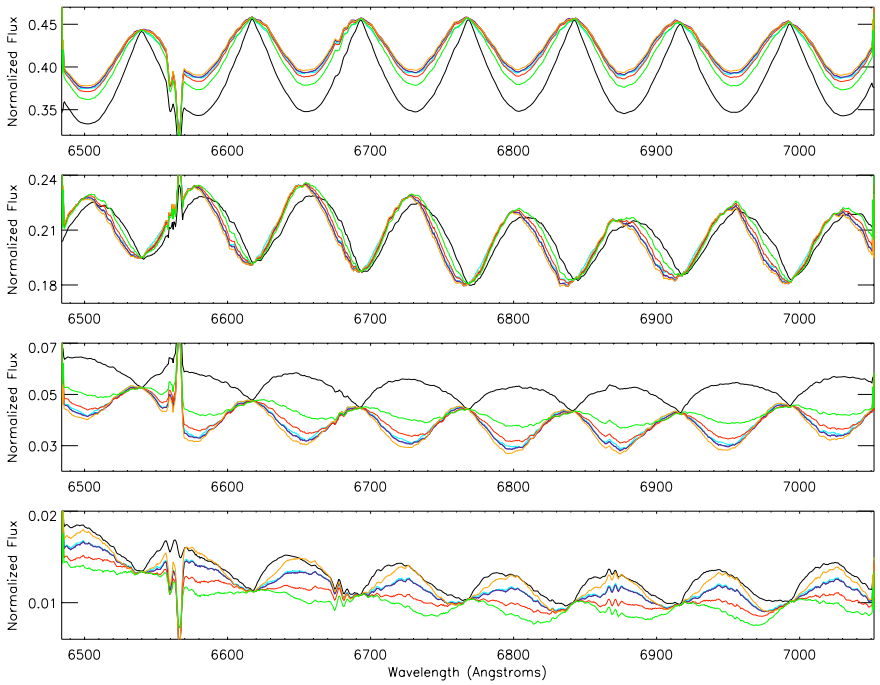

Figure 9: Spectra from Figure 7 rescaled to show structure better.

x2d image. For all but the lowest order fit, the fluctuations in that row are about 13% of the maximum flux in the wx2d images, and about 24% of the maximum flux in the x2d image. The fluctuations in the central row of the x2d image have sharper peaks, which may have more influence on the fitting of spectral lines in the vicinity of the peaks. The fluctuation patterns are obvious in the case of a point source, especially if the spectrum is fairly featureless or if it has been divided out, but they can be obscured in the scientifically interesting case of a region that is spatially and spectrally complex, with embedded compact continuum sources and/or embedded compact emission line sources. Obscured undersampling patterns are especially a problem for the M gratings, which have a short spectral baseline, when the central wavelength is set to cover a region full of spectral structure. Spectral "features" due to undersampling can be blended with real spectral features. If spectral fitting of the peak row is important, the reduced amplitude and smaller gradient in the spurious features in wx2d images is advantageous. One row off peak in either direction, the fluctuations in all of the wx2d spectra and the x2d spectra of the star are similar. At two or three rows out, the percentage fluctuations in the wx2d spectra can be as great as or greater than those in the x2d spectra. However, for a point source, the total amplitude of the flux in these rows is well down from the flux in the central row. The spatially extended component of interest in a science exposure will often dominate the compact component this far off the peak of the compact component.

6.2 Dependence of Artificial Spectral Structure on Target Placement

The artificial structure produced by resampling is sensitive to the placement of the target along the slit on the subpixel level. The exposure o5dh01010 of Beta Lyrae discussed above was followed by exposure o5dh01020, made with a displacement of 0.025 arcsec (half a CCD pixel) along the slit. SHIFTA2 was the same for the two exposures, so this displacement is preserved in x2d and wx2d images. SHIFTA2 fortuitously centered the resampled spectrum of o5dh01010 on a row. It therefore centered the resampled spectrum of o5dh01020 between two rows. Figures 10 and 11 show the 3 adjacent rows below the center and above the center of the spectrum, respectively, for the x2d image (black lines) and the wx2d image (polynomial order 7, subpixel 8; blue lines). As for Figures 6 and 7 for exposure o5dh01010, the spectrum summed over 21 rows has been divided out to better show the pattern resulting from resampling undersampled spatial structure. wx2d places somewhat more flux in the two most central rows than x2d, but the artificial structure and percentage fluctuations are comparable. wx2d produces the greatest differences from x2d when the spectrum in the resampled images is centered on a row.

Note that there is no difference in the counts collected in a column when the PSF is centered on a row and when it is centered between rows. The profiles along columns differ because of the shift in centering (and secondary effects like charge diffusion and CTE tails), not because of light loss at the edges of pixels. When 21 rows of the crj images of exposures o5dh01010 and o5dh01020 are summed into spectra, the ratio of the counts in the spectra is 1.001 +/- 0.004.

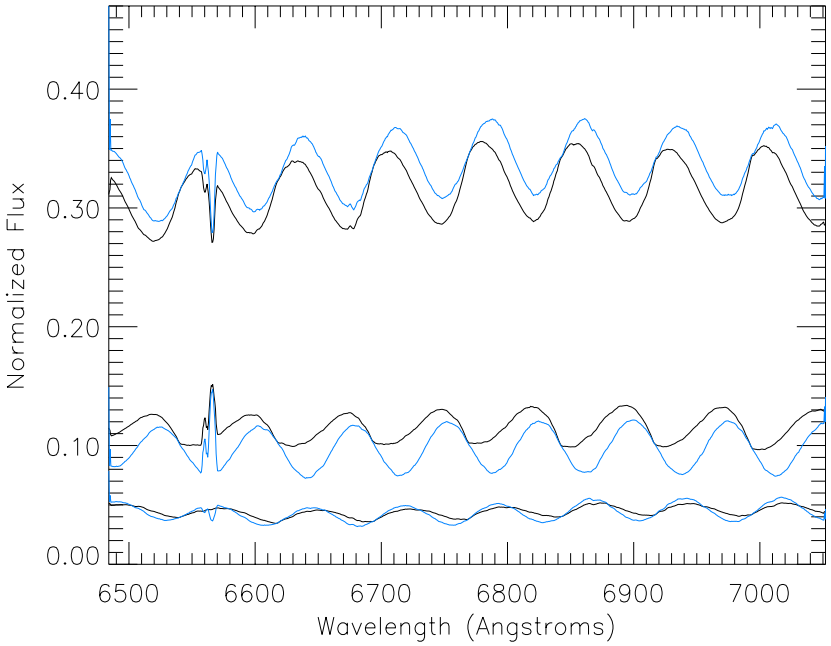

Figure 10: Spectra of the 3 rows just below the trace center of o5dh01020 (offset by 0.5 pixel along the slit from o5dh01020, shown in the previous figures), normalized by the spectrum summed over 21 rows. Reductions using x2d (black) and wx2d for parameters o7s8 (blue) are shown, where oN indicates fitting with an Nth order polynomial and sN indicates dividing pixels into N subpixels.

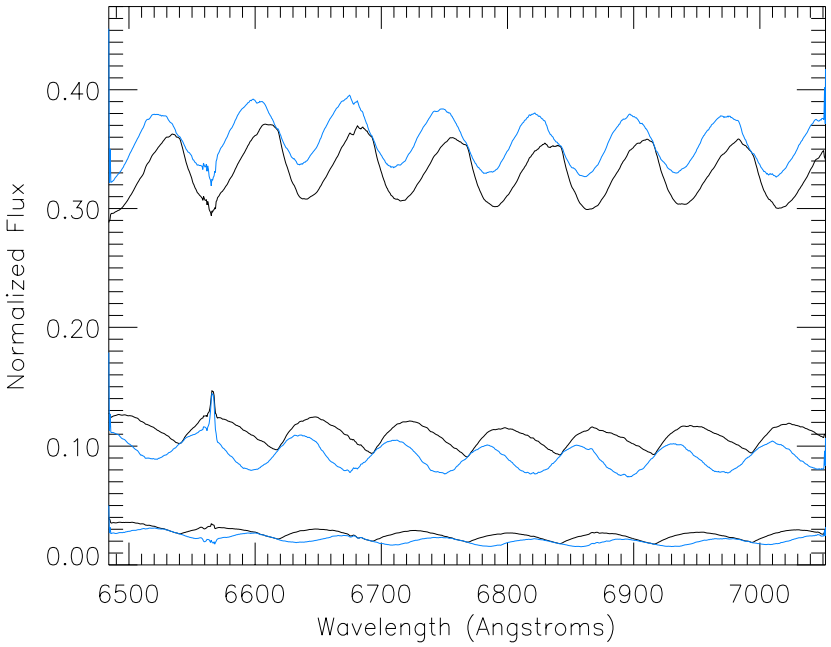

Figure 11: Analogous to Figure 10 for the 3 rows just above the trace center.

6.3 Dependence of Artificial Spectral Structure on SHIFTA2

The artificial structure produced by resampling is sensitive to the shift along the slit introduced by SHIFTA2. To illustrate this, we used the routine hedit to increase SHIFTA2 by 0.5 pixels before resampling the crj image of the second exposure of Beta Lyrae, o5dh01020. This causes the spectrum in the resampled image to be centered 0.5 pixels lower, at the same location as the spectrum in the resampled image of the first exposure, o5dh01010. Figures 12 and 13 show the central row and the 3 adjacent rows below the center and above the center of the spectrum, respectively, for the x2d image (black lines) and the wx2d image (polynomial order 7, subpixel 8; blue lines). As before, the spectrum summed over 21 rows has been divided out. The normalized spectra in these figures are very similar to the analogous spectra in Figures 6 and 7, except for a phase shift. The sets of columns where the flux profile is well centered (and therefore strongly peaked) in the two crj images are out of phase by half the cycle of the artifact pattern, and this spacing is preserved in the spacing of the peak flux columns in the resampled images.

6.4 Reduction of Artifacts by Convolution and Summation

The magnitude of spectral artifacts near the spatial peak of a point source can be reduced by using convolution in wx2d or by summing rows in the resampled image. The convolution kernel that approximates the spatial PSF in CCD spectral images, with wx2d parameter width = 1.3, is shown as a blue line in Figure 14. The "equivalent width" of this kernel is 2 pixels, denoted by the red line. Convolution provides better spatial resolution at the peak of the PSF than the summation of 2 rows, but contaminates the spectrum with flux from further out. This, of course, is relevant when dealing with images of a combination of spatial components with different spectra.

Here we examine the spectral artifacts in the peak row of a wx2d spectral image made with convolution and the artifacts in the summation of 2 rows from an unconvolved wx2d image and an x2d image. The convolution is applied to exposure o5dh01020 of Beta Lyrae after incrementing the value of SHIFTA2 by 0.5 pixel to center the resampled spectrum on a row. The summation is performed on resampled images made from that same exposure using the original value of SHIFTA2, which centers the spectrum between the two rows that will be summed. The default values of polynomial order (7) and number of subpixels (8) are used in wx2d. The spectrum summed over 21 rows is divided out to show the artifacts. Figure 15 shows the peak row of the convolved wx2d image (blue line), the combined (averaged) two center-most rows in the unconvolved wx2d image (red line), and the combined (averaged) two center-most rows in the x2d image (black line). The convolved and combined-row wx2d spectra have comparable fluctuations (3% and 2%, respectively), which are much smaller than the fluctuations in the combined-row x2d spectrum (10%).

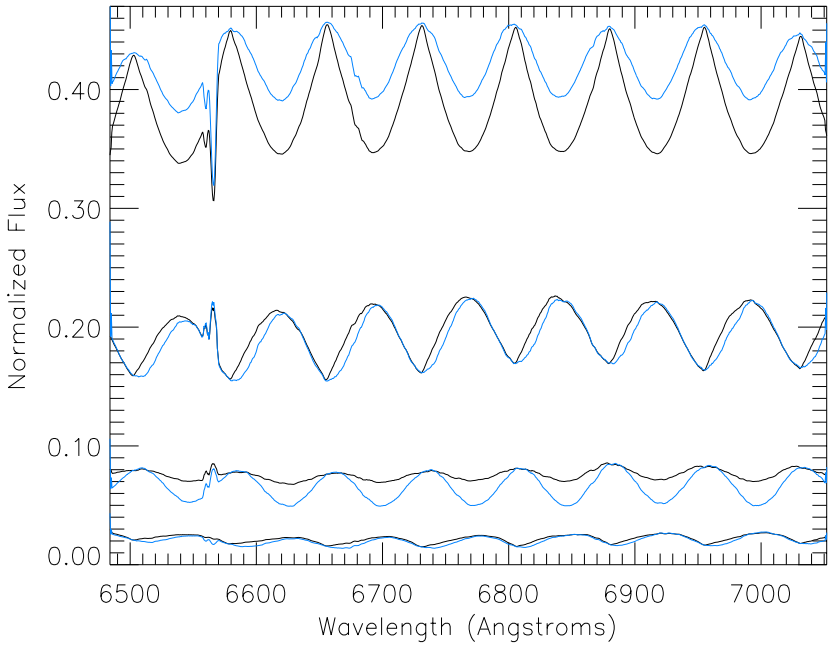

Figure 12: Spectrum in the peak row of o5dh01020 and the next 3 rows down, normalized by the spectrum summed over 21 rows. SHIFTA2 was incremented by 0.5 pixels to cause the spectrum to be centered on a row in the resampled image. Reductions using x2d (black) and wx2d for parameters o7s8 (blue) are shown, where oN indicates fitting with an Nth order polynomial and sN indicates dividing pixels into N subpixels.

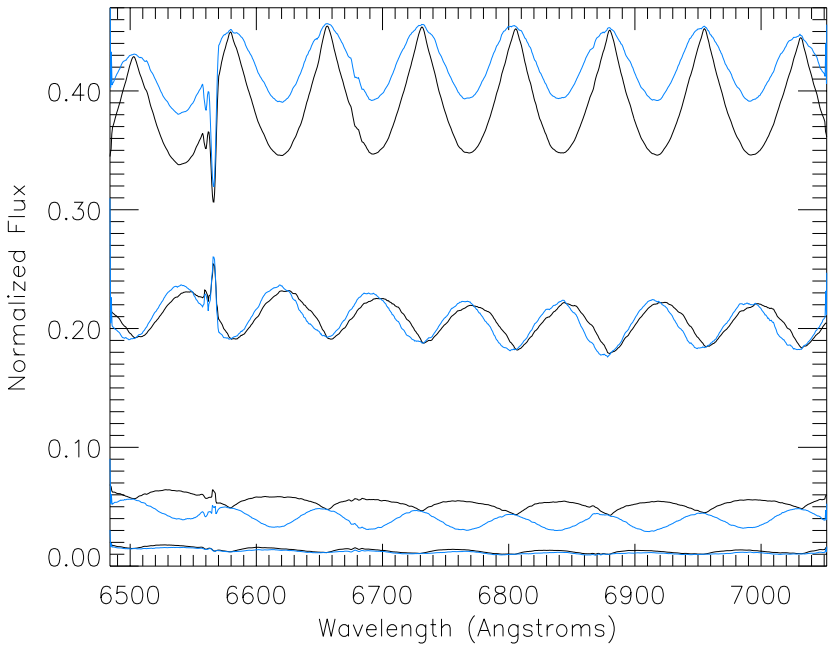

Figure 13: Analogous to Figure 12 for the peak row of o5dh01020 (with SHIFTA2 incremented by 0.5 pixels) and the next 3 rows up.

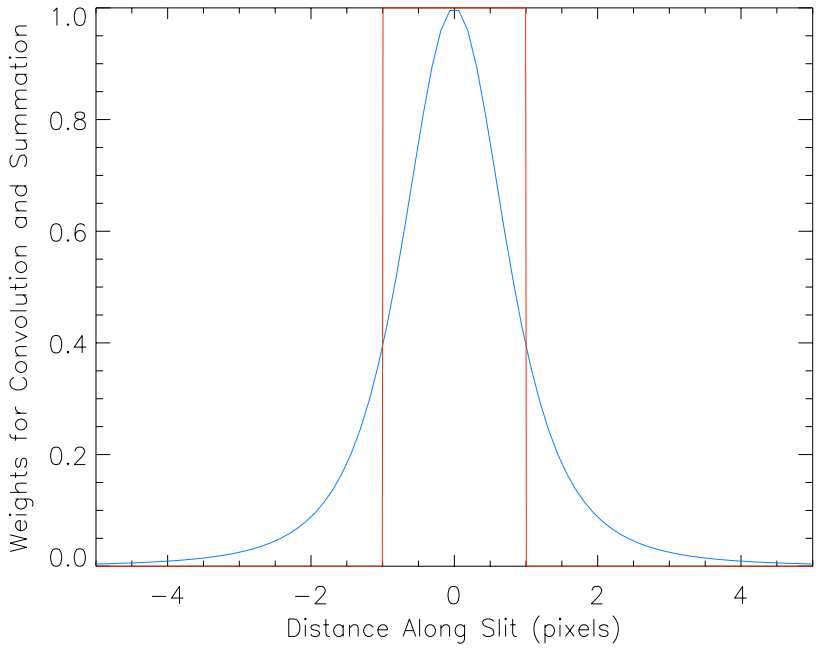

Figure 14: Convolution function to be applied in wx2d (blue) and summation to be applied to unconvolved wx2d image and x2d image. (See Figure 15.)

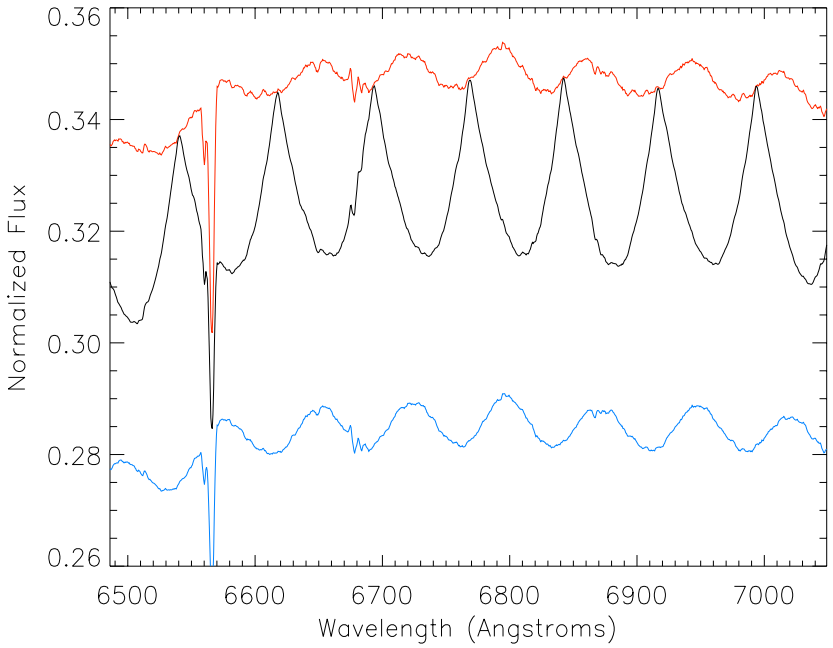

Figure 15: Peak row of the convolved wx2d image (blue), the combined (averaged) two center-most rows in the unconvolved wx2d image (red), and the combined (averaged) two center-most rows in the x2d image (black) for o5dh01020. The spectrum summed over 21 rows has been divided out to show the structure of the artifacts.

7. Conclusion

Resampling of STIS spectral images to align rows with traces necessarily produces errors in the spectral rows when point sources are present because the STIS detectors (especially the CCD detector) undersample the spatial point spread function. For an isolated point source with a relatively featureless spectrum, the signature of the undersampling is especially apparent if the trace drops by many pixels as it crosses the detector, resulting in periodic fluctuations in each spectral row of the resampled image. For spatially and spectrally complex targets that contain compact components, the modulation of the spectra of the compact components can be blended with real spectral features that change from row to row, affecting the measurement of those features. Here we have presented the PyRAF/STSDAS routine wx2d as an alternative to the STSDAS routine x2d for resampling spectral images. We have shown that wx2d produces modulation of smaller amplitude and with less sharply peaked periodic patterns for the peak flux row of a compact component in the resampled image. When the option of spatial convolution with a PSF kernel is used, or when two rows straddling the position of the compact source are combined, the modulation is further reduced, and is less than the modulation in a combined pair of rows from an x2d image. The impact of undersampling-induced spectral artifacts must be weighed against the need for spatial resolution when deciding whether to use either convolution or summation of rows to reduce the magnitude of the artifacts.

This report has shown the limitations of attempting to compensate for undersampling by the use of better mathematical techniques. The best way to produce STIS direct or spectral images with high spatial resolution is to improve the sampling by taking fractional pixel dither steps in the spatial dimension(s). Even a single half-pixel dither greatly improves the sampling of the PSF by the CCD, the detector with the poorest sampling. Note that a half-pixel dither along the slit would not necessarily require doubling the observing time, since the improved sampling is needed only for the compact components. For spectral imaging of a strong compact component blended with faint diffuse emission, it may suffice to take a long exposure at one position to get good signal-to-noise on both the compact component and the diffuse emission and a short exposure at the other position to get good signal-to-noise on the compact component only. (Both exposures should be CR-SPLIT, or include a dither of N pixels so that hot pixels can be rejected along with cosmic rays.) At present, MultiDrizzle can be applied to dithered STIS direct imaging exposures, but spectroscopic MultiDrizzle has not been implemented. If STIS is repaired as planned, software priorities will be reassessed.

Acknowledgments

We thank Paul Goudfrooij for his involvement in the early stages of this project. We thank Mary Beth Kaiser and Charles Proffitt for reviewing this manuscript.

References

Barrett, P. and Dressel, L., 2005, "Spectral Extraction of Extended Sources Using Wavelet Interpolation", in The HST Calibration Workshop: Hubble After the Transition to Two-Gyro Mode, ed. A. M. Koekemoer, P. Goudfrooij, & L. Dressel, p. 260.

Davidson, K., 2005, "Some Neglected Pixel Problems", in The HST Calibration Workshop: Hubble After the Transition to Two-Gyro Mode, ed. A. M. Koekemoer, P. Goudfrooij, & L. Dressel, p. 247.

Dressel, L., STIS Instrument Science Report 2006-02, "Spectroscopic PSF: Comparison of Data and Models for a Target Centered in and Out of the Aperture".

Dressel, L., Bohlin, R., Lindler, D. & Holfeltz, S., STIS Instrument Science Report 2007-03, "Time Dependent Trace Angles for the STIS First Order Modes".

Dressel, L., Holfeltz, S., & Kim Quijano, J. 2007, STIS Data Handbook, Version 5.0, (Baltimore: STScI).